

Classical fields in the one-dimensional Bose gas: applicability and determination of the optimal cutoff

J. Pietraszewicz¹ and P. Deuar¹

¹*Institute of Physics, Polish Academy of Sciences, Aleja Lotników 32/46, 02-668 Warsaw, Poland**

(Dated: December 9, 2021)

To finalize information about the accuracy of the classical field approach for the 1d Bose gas, the lowest temperature quasicondensate was studied by comparing the extended Bogoliubov model of Mora and Castin, to its classical field analogue. The parameters for which the physics is well described by matter waves are now presented for all 1d regimes, and concurrently, the optimal cutoff that best matches all observables together is also provided. This cutoff rises strongly with density when the chemical potential is higher than the thermal energy to account for kinetic energy. As a consequence, clouds that reach this coldest quantum fluctuating regime are better described using a trap basis than plane waves. This contrasts with higher temperature clouds for which the basis choice is less important. In passing, estimates for chemical potential, density fluctuations, kinetic and interaction energy in the low temperature quasicondensate are obtained up to several leading terms.

I. INTRODUCTION

The question of under what conditions the classical field description of ultracold gases is accurate has been widely discussed in the field [1–13]. In parallel, the companion question is what high energy cutoff should be chosen for best results [7, 9, 12–20]. The importance of these matters stems from the widespread utility of the method for nonperturbative and thermal calculations [1, 8, 11, 21–32] and its interpretation in terms of matter waves.

Previous work in the 1d Bose gas gave detailed quantitative answers to these questions for most degenerate temperatures [12, 13], by comparing classical field ensembles with the exact Yang-Yang results [33–35]. However, the full picture was not obtained because there were technical difficulties in assessing the colder quasicondensate for which quantum fluctuations become significant. In practice this meant that when thermal energy $k_B T$ is comparable to or lower than the chemical potential, the status of the classical field description of the centre of a gas cloud was unclear.

Here, to obtain complete coverage, we re-analyze the case of the quasicondensate by comparing the extended Bogoliubov theory of Mora and Castin [36] with its classical field counterpart [37]. The present analysis conforms with the previous results but also extends the determinations down to zero temperature. In this way, a comprehensive assessment across all regimes of the 1d Bose gas is now provided in this work.

The structure of the paper is as follows: Sec. II gives the background information, while Sec. III describes the extended Bogoliubov description and its classical field version that we will use to study the quasicondensate. Sec. IV explains how classical field accuracy will be

judged there. Sec. V compares full quantum and classical field predictions and gives the main results, i.e. the limits of the matter wave region and the optimal cutoff prescription. Sec. VI discusses the physical reasons for the high cutoff found in the quantum fluctuating region, and its consequences. We summarize in Sec. VII. Additional technical details are given in the appendices, as well as a number of analytic estimates for the main observables in the Bogoliubov regime.

II. BACKGROUND

The interest in a precise characterization of the classical field description is twofold.

The *practical aspect* is the usage of the classical field method to simulate dynamics. Many kinds of non-perturbative phenomena have become accessible experimentally in recent years [30, 31, 38–40], but in a vast range of cases, only classical fields remain tractable for very large systems. Furthermore, they also give access to predictions for single experimental runs [1, 2, 4, 8, 21, 41–44]. Several flavors of c-fields have been developed [6, 8, 17, 45, 46] and applied to defect seeding and formation [23, 25, 27, 30, 47–51], quantum turbulence [31, 52–54], the Kibble-Zurek mechanism [26, 55–57], nonthermal fixed points [58–61], vortex dynamics [18, 49, 62], the BKT transition [49], evaporative cooling [25, 32, 63, 64], and more.

All c-field varieties tend to suffer from ambiguity regarding the best choice of high-energy cutoff, because predictions of observables can depend sizeably on the cutoff choice. A range of prescriptions for choosing cutoff have been developed [8, 9, 12–16, 18, 20, 37, 65] but generally no particular choice is ideal. For example, a cutoff that leads to correct predictions of density and one additional observable will inaccurately describe other quantities [13].

The *physical aspect* of characterizing “classical” field

* pietras@ifpan.edu.pl, deuar@ifpan.edu.pl

descriptions is that they describe the physics of matter waves, while neglecting effects due to particle discretization. In the ultracold atom domain this is not at all the same as so-called *classical physics*. However, it does mean that wave-particle duality is insignificant whenever a classical field description is good. Hence, by studying its accuracy, one can show the regimes in which wave-particle duality is relevant or not.

Quantitative studies were begun in [12, 13] and are continued here. A figure of merit minRMS , first identified in [13], bounds the discrepancy in all the standard observables, and provides a cutoff value $\text{opt}f_c$ that minimizes inaccuracies. A good classical wave description will only be present if there is some cutoff choice that leads to small discrepancy in *all* the relevant observables simultaneously. Below 10% is a reasonable value, since experimental precision is also of this order.

As in the analyses of [12, 13], we will consider locally uniform sections of the 1d gas in the grand canonical ensemble. The latter corresponds to thermal and diffusive contact between neighboring sections. Such assumptions enable wider usage of the results for non-uniform gases via a local density approach. We also assume that the gas sections are large enough to be in the thermodynamic limit with regard to the observables that will be considered. In the Bogoliubov region, the limiting ones are kinetic energy ε and the phase coherence.

Such a uniform 1d Bose gas section is fully characterized by only two parameters: The dimensionless interaction strength γ and dimensionless temperature τ_d :

$$\gamma = \frac{mg}{\hbar^2 n}; \quad \tau_d = \frac{T}{T_d} = \frac{1}{2\pi} \frac{mk_B T}{\hbar^2 n^2}. \quad (1)$$

Here n is the density, T the temperature, m the particle mass, and g the contact interaction strength. When temperature reaches the quantum degeneracy temperature T_d , there is about one particle per thermal de Broglie wavelength $\Lambda_T = \sqrt{\frac{2\pi\hbar^2}{mk_B T}}$.

The physical regime that is particularly relevant for the analysis here is the *quasicondensate* lying in the range $\tau_d^2 \lesssim \gamma \lesssim 1$ in which density fluctuations are small, and the relation

$$\mu \approx k_B T \frac{\gamma}{2\pi\tau_d} \quad (2)$$

holds. The quasicondensate consists of two physically different regions characterized by the dominance of either:

- *Thermal fluctuations* when $k_B T \gtrsim \mu$, or
- *Quantum fluctuations* when $k_B T \lesssim \mu$.

This distinction makes a large difference for classical field accuracy and cutoff dependence.

Low temperatures with $k_B T \lesssim \mu$ were difficult to access using the methods employed previously [13]. Convergence to the equilibrium state in the thermodynamic

limit became very slow there, both for the iterative algorithm that is used to solve the Yang-Yang integral equations, and also for the generation of classical field ensembles via Metropolis [66] or SPGPE [46]. This slowness was compounded by the growth of the numerical lattices as temperature falls.

III. QUASICONDENSATE DESCRIPTION

The quasicondensate is very well described by the extended Bogoliubov model given by Mora and Castin [36], across a wide range of temperatures. The model does not assume a single phase-coherent dominant condensate mode like standard Bogoliubov [67, 68], but makes an expansion in small density fluctuations instead. Section III A summarizes the resulting fully quantum description for the uniform gas which will be our baseline for comparison, while Sec. III B describes the corresponding classical field description.

A. Extended Bogoliubov model for a uniform 1d gas

The boson field $\hat{\Psi}(x)$ in this model is expressed as

$$\hat{\Psi}(x) = e^{i\hat{\theta}(x)} \sqrt{\hat{\rho}(x)}, \quad \hat{\rho}(x) = \rho_0 + \delta\hat{\rho}(x), \quad (3)$$

with the help of operators for the phase $\hat{\theta}(x)$ and density fluctuations $\delta\hat{\rho}(x)$. The quantity ρ_0 is the lowest order density estimate obtained from the Gross-Pitaevskii solution. The gas section of length L is discretized into sites of length Δx . Two small parameters are assumed: $|\delta\hat{\rho}(x)| \ll \rho_0$ (which makes this a quasicondensate), and $|\hat{\theta}(x + \Delta x) - \hat{\theta}(x)| \ll 1$ (which is needed to ensure that the discretization of space corresponds to the continuum model). The latter is needed to self-consistently define the operator $\hat{\theta}$ in (3). The exact quantum model is then truncated to 2nd or 3rd order in these small parameters, as the situation warrants, and the Hamiltonian takes the form

$$\hat{H} = \sum_{k \neq 0} E_k \hat{b}_k^\dagger \hat{b}_k + \frac{g}{2L} \hat{P}^2 + E_{\text{ground}}. \quad (4)$$

The \hat{b}_k (\hat{b}_k^\dagger) are quasiparticle annihilation (creation) operators for excited plane wave modes, with the usual commutation relation $[\hat{b}_k, \hat{b}_{k'}^\dagger] = \delta_{kk'}$. The system's description resembles an ideal gas of Bogoliubov quasiparticles. The quasiparticle energy is

$$E_k = \sqrt{\epsilon_k(\epsilon_k + 2\mu)}, \quad (5)$$

in terms of the free-particle energy $\epsilon_k = \frac{\hbar^2 k^2}{2m}$ and chemical potential μ . The $k = 0$ mode is represented by the background density ρ_0 , while \hat{P} is a dimensionless operator related to fluctuations in the total number of particles. There is also an operator \hat{Q} , which is a zero energy

collective coordinate for the global quantum phase. Both commute with all \hat{b}_k and \hat{b}_k^\dagger and, moreover satisfy the relation $[\hat{P}, \hat{Q}] = -i$.

To evaluate observables, the wavefunction elements in (3) can be expanded as:

$$\begin{aligned}\delta\hat{\rho}(x) &= \sqrt{\frac{\rho_0}{L}} \sum_{k \neq 0} (\bar{u}_k + \bar{v}_k) \left[e^{ikx} \hat{b}_k + e^{-ikx} \hat{b}_k^\dagger \right] + \frac{\hat{P}}{L} \\ \hat{\theta}(x) &= \frac{1}{2i\sqrt{\rho_0 L}} \sum_{k \neq 0} (\bar{u}_k - \bar{v}_k) \left[e^{ikx} \hat{b}_k - e^{-ikx} \hat{b}_k^\dagger \right] - \hat{Q}\end{aligned}\quad (6)$$

where the quasiparticle wavefunction amplitudes are

$$\bar{u}_k \pm \bar{v}_k = \left[\frac{\epsilon_k}{\epsilon_k + 2\mu} \right]^{\pm 1/4}. \quad (7)$$

In thermal equilibrium all single operators $\hat{b}_k, \hat{b}_k^\dagger, \hat{P}$ and the anomalous average $\hat{b}_k \hat{b}_{k'}$ have zero mean, except for the occupations $\langle \hat{b}_k^\dagger \hat{b}_{k'} \rangle = \delta_{kk'} n_k$, which are Bose-Einstein distributed:

$$n_k = \frac{1}{e^{E_k/k_B T} - 1}. \quad (8)$$

Also, $\langle \hat{P}^2 \rangle = k_B T \frac{L}{g}$. Averages involving \hat{Q} are usually unnecessary.

In the thermodynamic limit, the sum $\sum_{k \neq 0}$ can be replaced¹ by $\frac{L}{2\pi} \int_{-\infty}^{\infty} dk$. Under the above circumstances the equation of state is given by an integral:

$$n = \frac{\mu}{g} - \int_{-\infty}^{\infty} \frac{dk}{2\pi} [(\bar{u}_k + \bar{v}_k)^2 n_k + \bar{v}_k (\bar{u}_k + \bar{v}_k)]. \quad (9)$$

This allows one to retroactively obtain $\mu/k_B T$ at given γ and τ_d values. They determine g and n via (1), apart from the one free scaling parameter $k_B T$. Observables written in terms of $\hat{\Psi}(x)$ can then be explicitly evaluated (see Appendix B 1 for expressions).

B. Classical field in the Bogoliubov regime

Let us now construct the classical field analogue for the extended Bogoliubov model. In general, a Bose field can be written in terms of mode functions $\psi_j(\mathbf{x})$ and mode annihilation operators \hat{a}_j as

$$\hat{\Psi}(\mathbf{x}) = \sum_j \hat{a}_j \psi_j(\mathbf{x}). \quad (10)$$

The underlying idea of classical field descriptions is that the creation/annihilation operators $\hat{a}_j^\dagger, \hat{a}_j$ of highly occupied modes can be quite well approximated by complex amplitudes $\alpha_j \approx \hat{a}_j$. This is because for a highly occupied mode with $\bar{n}_j = \langle \hat{a}_j^\dagger \hat{a}_j \rangle$, the commutator $[\hat{a}_j, \hat{a}_j^\dagger] \approx \mathcal{O}(1)$ is much smaller than $\sqrt{\bar{n}_j}$. The Bose field can then be approximated as

$$\hat{\Psi}(\mathbf{x}) \rightarrow \Psi(\mathbf{x}) = \sum_{j \in \mathcal{C}} \alpha_j \psi_j(\mathbf{x}). \quad (11)$$

For in-depth discussion of classical fields, we refer the reader to [1–4] and the earlier reviews [6, 8, 45].

The c-field approximation corresponding to the extended Bogoliubov model is constructed using the quasiparticle modes \hat{b}_k in place of the \hat{a}_j . In the uniform case these modes are plane waves with wavevector $k = 2\pi j/L$. Several changes with respect to Sec. III A need to be introduced to obtain the c-field description:

1. The approximation (11) breaks down for high energy modes, since they will be poorly occupied. For this reason, the available set of modes should be restricted to a subspace \mathcal{C} specified by an energy cutoff E_c . In a uniform system, E_c is equivalent to a certain cutoff wavevector k_c such that $0 < |k| \leq k_c$. At the cutoff, the kinetic energy is $\epsilon_c = \hbar^2 k_c^2 / 2m$, and in the particle-like regime above phonon excitations $E_c \approx \epsilon_c$. Using the scaling of (1) with respect to the thermal de Broglie wavelength Λ_T , one can express k_c in dimensionless form:
2. The operators \hat{b}_k are replaced by appropriate random complex numbers b_k , that will give the required ensemble averages. The operator \hat{P} is replaced by random real values P with variance $k_B T \frac{L}{g}$, which preserve its average, and \hat{Q} by a real phase Q uniformly distributed on $[0, 2\pi)$.
3. Quantum expectation values of operators $\langle \cdot \rangle$ are replaced by stochastic averages $\langle \cdot \rangle_s$ of c-field amplitudes.

The change from operators to c-numbers requires some care. Firstly, since we want to compare thermal equilibrium states, we should keep in mind that c-fields equilibrate to Rayleigh-Jeans occupations, not Bose-Einstein. The correct thermal averages to use are then $\langle b_k^\dagger b_{k'} \rangle_s = \delta_{kk'} n_k^{(\text{cf})}$, with

$$n_k^{(\text{cf})} = \frac{k_B T}{E_k} \quad (13)$$

and $\langle b_k b_{k'} \rangle_s = 0$. Means $\langle b_k \rangle_s$ and $\langle P \rangle_s$ remain zero.

Secondly, now b_k and b_k^* commute, so that some observable expressions in thermal equilibrium need to be

¹ This is notwithstanding the fact that the theory in [36] is written in terms of a fine discretization of space with spacing Δx . This formally corresponds to $\int_{-\pi/\Delta x}^{\pi/\Delta x}$, but for any well described physical quantity the result must be unchanged in the limit $\Delta x \rightarrow 0$.

slightly modified. For example, $\langle b_k b_k^* \rangle_s = \langle b_k^* b_k \rangle_s = n_k^{(\text{cf})}$, in contrast to $\langle \hat{b}_k \hat{b}_k^\dagger \rangle = \langle \hat{b}_k^\dagger \hat{b}_k \rangle + 1$.

In the thermodynamic limit, applying the above changes, (6) transform to:

$$\begin{aligned}\delta\hat{\rho}(x) &\rightarrow \frac{\sqrt{L\rho_0}}{2\pi} \int_{-k_c}^{k_c} dk (\bar{u}_k + \bar{v}_k) [e^{ikx} b_k + e^{-ikx} b_k^*] + \frac{P}{L} \\ \hat{\theta}(x) &\rightarrow \frac{\sqrt{L}}{4i\pi\sqrt{\rho_0}} \int_{-k_c}^{k_c} dk (\bar{u}_k - \bar{v}_k) [e^{ikx} b_k - e^{-ikx} b_k^*] - Q.\end{aligned}\quad (14)$$

The equation of state for classical fields becomes

$$n = \frac{\mu^{(\text{cf})}(k_c)}{g} - \int_{-k_c}^{k_c} \frac{dk}{2\pi} (\bar{u}_k + \bar{v}_k)^2 n_k^{(\text{cf})}. \quad (15)$$

The chemical potential for a given density n is different than the quantum one, and depends on the cutoff. That is, $\mu \rightarrow \mu^{(\text{cf})}(k_c)$ when evaluating $\bar{u}_k, \bar{v}_k, n_k^{(\text{cf})}$ or E_k .

Further quantities can be obtained using the same sequence of steps. as in [36]. The local density-density correlation $g^{(2)}(z) = \frac{1}{n^2} \langle \hat{\Psi}^\dagger(x) \hat{\Psi}^\dagger(x+z) \hat{\Psi}(x+z) \hat{\Psi}(x) \rangle$ is expressed as

$$g_{\text{cf}}^{(2)}(z) = 1 + \frac{2}{n} \int_{-k_c}^{k_c} \frac{dk}{2\pi} (\bar{u}_k + \bar{v}_k)^2 n_k^{(\text{cf})} \cos kz. \quad (16)$$

The coarse-grained density fluctuations in imaging bins measured in experiments [69–74] are

$$u_G := \frac{\text{var}\hat{N}}{\langle \hat{N} \rangle} \quad (17)$$

so, substituting the Bogoliubov expressions, one obtains

$$u_G^{\text{cf}} = 2 \lim_{k \rightarrow 0} (\bar{u}_k + \bar{v}_k)^2 n_k^{(\text{cf})} = \frac{k_B T}{\mu^{(\text{cf})}(k_c)}. \quad (18)$$

The interaction energy per particle is trivially related to $g^{(2)}(0)$ straight from the Hamiltonian:

$$\mathcal{E}_{\text{int}} = \frac{gn}{2} g_{\text{cf}}^{(2)}(0) = \mu^{(\text{cf})}(k_c) - k_B T \frac{\gamma}{4\pi\tau_d}. \quad (19)$$

The kinetic energy per particle is

$$\varepsilon = \frac{\hbar^2}{2mn} \int_{-k_c}^{k_c} \frac{dk}{2\pi} k^2 (1 + 2\bar{v}_k^2) n_k^{(\text{cf})} \quad (20)$$

and the total energy is $\mathcal{E}_{\text{tot}} = \mathcal{E}_{\text{int}} + \varepsilon$. Some additional expressions are given in Appendix. B 1.

IV. ACCURACY INDICATOR

The observables studied at hotter temperatures [12, 13] were the local density fluctuations $g^{(2)}(z)$, coarse grained density fluctuations u_G and the kinetic ε , interaction \mathcal{E}_{int} ,

and total \mathcal{E}_{tot} energies. It was confirmed that three quantities ($u_G, \varepsilon, \mathcal{E}_{\text{tot}}$) suffice to produce a bound on the maximum deviation between c-field and exact predictions. The discrepancies in all the other observables were consistently smaller. Based on this observation, the maximum global error was defined as

$$RMS(\gamma, \tau_d, f_c) = \sqrt{\left(\delta_{u_G}\right)^2 + \max\left[\delta_\varepsilon^2, \delta_{\mathcal{E}_{\text{tot}}}^2\right]}, \quad (21)$$

with the relative error δ_Ω for a given observable Ω .

We follow the same route here. The relative errors are

$$\delta_\Omega = \left[\frac{\Omega^{(\text{Bog-cf})}(\gamma, \tau_d, f_c)}{\Omega^{(\text{Bog-q})}(\gamma, \tau_d)} - 1 \right], \quad (22)$$

where the fully quantum value is $\Omega^{(\text{Bog-q})}$ and the classical field value is $\Omega^{(\text{Bog-cf})}$. When comparing, we set the density n in fully quantum and c-field results to be equal, so that they correspond to the same values of the γ and τ_d parameters.

In the colder quasicondensate, we have checked for various parameter values that the three quantities used in (21) continue to have the largest errors compared to other observables. (A representative case is shown in Fig. 6 in Appendix B 2). In this way we confirm that (21) is an adequate indicator of c-field accuracy in the entire quasicondensate regime.

The minimum of RMS , $\text{min}RMS$ gives a figure of merit for the classical field description, and the value $f_c = \text{opt}f_c$ at which it occurs, gives the best cutoff to use. Some analytic estimates are given in Sec. D.

V. THE COMPLETE CLASSICAL WAVE REGIME AND OPTIMAL CUTOFF TO USE

We have calculated $\text{min}RMS$ and $\text{opt}f_c$ in the entire quasicondensate regime by evaluating the appropriate integrals for observables. This supplements the earlier results for $k_B T \gtrsim \mu$. Figs. 1–2 show a synthesis of these data sets, and are our main results. It is pleasing to note the perfect compatibility (contact) between the red contours obtained from the Bogoliubov theory and the blue contours obtained previously [13]. Raw results are shown in Fig. 8 in Appendix. B 2.

Fig. 1 describes the **accuracy of the c-field description**. The light orange area in which accuracy is better than 10% covers all temperatures from $\tau_d = 0.008$ in the quantum degenerate region down to $T = 0$, and covers the whole dilute gas up to around $\gamma = 0.018$. It also extends somewhat further up to around $\tau_d \approx \gamma \approx 0.03$, for reasons that are not understood at the moment.

It can now be seen that all the low order observables remain well described in the quantum fluctuating region, even down to $T = 0$. This is something that was not obvious *a priori* since the weak antibunching that occurs due to quantum depletion ($g^{(2)}(0) \approx 1 - 2\sqrt{\gamma}/\pi$ [75, 76])

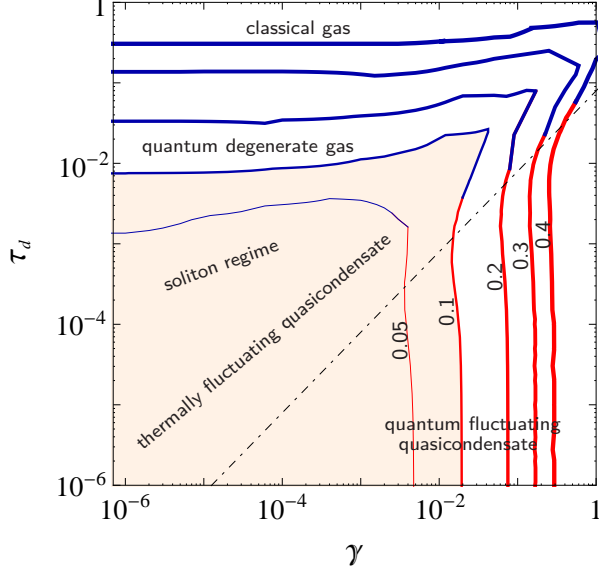


Figure 1. The regime of applicability for classical fields, shown in light orange. In this region, observables are accurate to 10% or better. The values of the minRMS indicator that bounds the accuracy are shown as a contour plot, with values printed on the figure. The blue contours are from [13], while the red lines are obtained with the extended Bogoliubov theory used here. The dot-dashed line indicates the location of the $\mu \sim k_B T$ crossover between quasicondensates dominated by thermal and quantum fluctuations.

cannot be correctly replicated by classical fields. However, this has little effect on the coarse-grained density fluctuation statistics

$$u_G = n \int d\mathbf{z} [g^{(2)}(\mathbf{z}) - 1] + 1. \quad (23)$$

The reason is that the two contributions to u_G that are missing in classical fields (shot noise “+1” and antibunching in $g^{(2)}$) cancel in the full quantum description. In the c-field description, $g_{\text{cf}}^{(2)}(z) = \langle |\Psi(x)|^2 |\Psi(x+z)|^2 \rangle_s / n^2$, and from the definition (17) the number fluctuations are related by

$$u_G^{\text{cf}} := n \int d\mathbf{z} [g_{\text{cf}}^{(2)}(\mathbf{z}) - 1]. \quad (24)$$

instead of (23). The shot noise “+1” term is no longer present, and values of u_G tending to zero can continue to be obtained despite $g_{\text{cf}}^{(2)}(z) > 1$.

In turn, the dependence of the **optimal cutoff** $\text{opt}f_c$ is shown in Fig. 2. The main standout feature is that there are different behaviors depending on whether $k_B T \gtrsim \mu$ or $k_B T \lesssim \mu$, with a changeover marked by the dot-dashed line near the $\text{opt}f_c = 1$ contour.

In the thermal upper part of the diagram studied already in [13], one has a practically constant $\text{opt}f_c =$

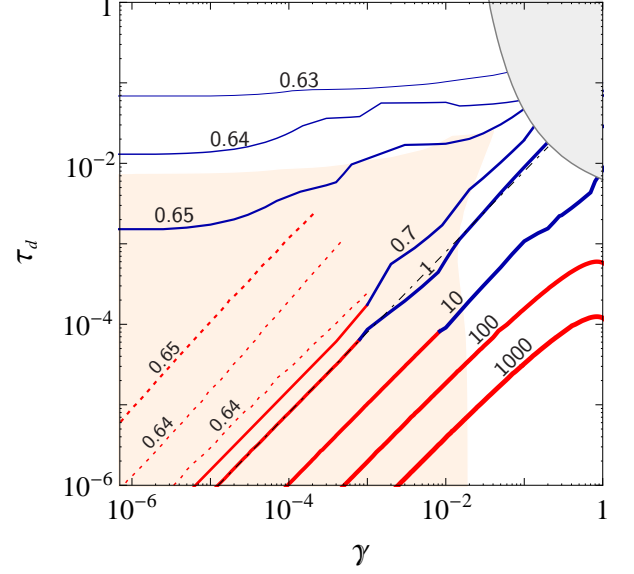


Figure 2. Globally optimal values of the cutoff $\text{opt}f_c$, shown with contours. Notation as in Fig. 1, and the light orange area indicates an accuracy of $\text{minRMS} < 0.1$. The gray colored area indicates a region from [13] in which there was insufficient precision in the numerical ensembles to determine the position of the closely spaced contours.

0.64 ± 0.01 , indicating that one cutoff choice is appropriate for the whole cloud when $k_B T \gtrsim \mu$. The Bogoliubov data (in red) also show this but are more precise at low temperatures. They indicate the presence of a broad shallow trough, between dashed red lines with values $\text{opt}f_c = 0.64$ in Fig. 2. The trough must disappear at higher temperatures since it was not seen in [13], while the correctness of the Bogoliubov decreases with growing temperature.

The lower part of Fig. 2 confirms the conjecture voiced in [13] that a change of cutoff behavior begins when quantum fluctuations dominate. A rapid growth of $\text{opt}f_c$ is observed, and approximated by

$$\text{opt}f_c = \frac{1}{12\pi^2} \left(\frac{\gamma}{\tau_d} \right)^{\frac{3}{2}} \left[1 - \frac{7\sqrt{\gamma}}{2\pi} + \frac{3\pi^2 \tau_d}{\gamma} + \dots \right]. \quad (25)$$

See Sec. D 3. Concurrently,

$$\text{minRMS} = \frac{\sqrt{5}\gamma}{\pi} \left[1 + \frac{\sqrt{\gamma}}{30\pi} + \pi^2 \frac{\tau_d}{\gamma} + \dots \right]. \quad (26)$$

The dependence $\gamma/\tau_d \propto gn/T$ means that the cutoff begins to strongly depend on density in this region. This suggests that a larger range of momenta k should be allowed in the center of the cloud than in the tails. A plane-wave basis does not provide such a possibility, but a harmonic oscillator basis does, as studied in [9]. Hence, unlike at higher temperatures, clouds whose central region reaches $\mu \gtrsim k_B T$ should use bases that take into account the trap shape.

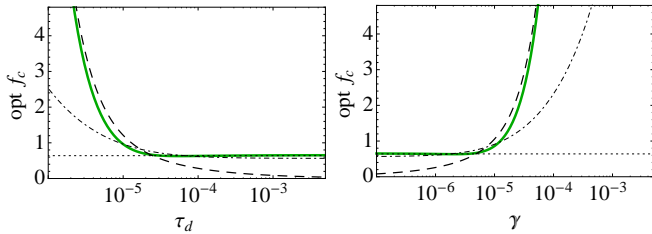


Figure 3. Optimal cutoff shown for two characteristic slices in parameter space (in green). Left panel: $\gamma = 1.2 \times 10^{-4}$. Right panel: $\tau = 10^{-6}$. The black lines show the two approximations: $\text{opt} f_c = 0.64$ – (dotted), (25) – (dashed), as well as the hitherto “rule of thumb” (27) (dot-dashed).

VI. KINETIC ENERGY AND PREVIOUS CUTOFF DETERMINATIONS

The reason why a high cutoff is needed in the low temperature quasicondensate is that the kinetic energy begins to rise steeply with γ . It can be shown that $\varepsilon \approx \frac{k_B T}{6\pi^2} \frac{\gamma^{3/2}}{\tau_d}$ there (see App. D).

The kinetic energy is contained in repulsive quantum fluctuations. In a c-field description quantum fluctuations are absent, so to build up the correct level of kinetic energy, extra modes (with $k_B T$ energy in each) should be introduced (details in App. C). Adding these extra modes does not adversely affect other important observables since their occupations are small.

The main cutoff result (25) can be compared to the widely used “rule of thumb” [4, 8, 77, 78]. This rule of thumb says that the single particle energy at the cutoff should be $\approx k_B T + \mu$, and for a plane-wave basis this energy is $\varepsilon_c = \pi(f_c)^2 k_B T$. Using (2) and (12) leads to:

$$f_c^{\text{thumb}} \approx \sqrt{\frac{1}{\pi} \left(\frac{\gamma}{2\pi\tau_d} + 1 \right)}. \quad (27)$$

Note that both (27) and (25) grow with the ratio γ/τ_d , but the global $\text{opt} f_c$ (25) grows with a faster power law. The difference can be seen in Fig. 3.

It is informative to look at the length scales allowed by the two cutoffs. The smallest length scale accessible with a k_c cutoff in a plane wave basis is about $\pi/k_c = \Lambda_T/2f_c$. For $k_B T \gtrsim \mu$ the accessible length scales reached up to the thermal de Broglie wavelength. However, for $k_B T \lesssim \mu$, one should resolve the healing length $\xi = \frac{\hbar}{\sqrt{m\mu}}$. The rule of thumb cutoff (27) leads to $\pi/k_c \approx \frac{\pi}{\sqrt{2}}\xi$, so that this resolution is achieved. In turn, the optimum cutoff (25) allows smaller length scales down to $\pi/k_c \approx 3\pi(\frac{k_B T}{\mu})\xi$.

In the history of the field, the cutoff has also been characterized by the c-field occupation N_c of the (quasi)particle mode with the highest energy [8, 16, 79]. It is expected that $N_c \sim 1$ from general arguments. In a

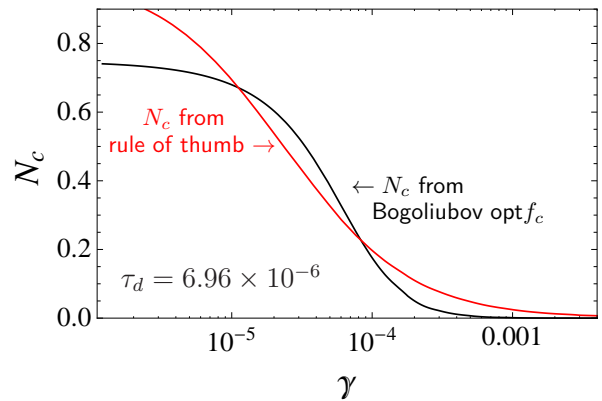


Figure 4. Occupation of the highest energy mode N_c when the cutoff is given by $\text{opt} f_c$ (black line) and the rule of thumb (27) (red line). The asymptotic value at low γ is 0.746.

Bogoliubov quasiparticle treatment one has

$$N_c \approx \frac{k_B T}{\sqrt{\varepsilon_c(\varepsilon_c + 2\mu)}}. \quad (28)$$

Fig. 4 presents the value corresponding to the numerically calculated $\text{opt} f_c$. Its analytic estimate for $k_B T \ll \mu$ is

$$N_c = 18 \left(\frac{2\pi\tau_d}{\gamma} \right)^3 \left[1 + \frac{7\sqrt{\gamma}}{\pi} - \frac{6\pi^2\tau_d}{\gamma} + \dots \right] \approx 18 \left(\frac{k_B T}{\mu} \right)^3. \quad (29)$$

At small γ , N_c takes the value 0.746. It initially looks surprising that N_c plummets to zero in the quantum fluctuating regime. However, the rule of thumb (27) also predicts a rapidly falling N_c behavior with γ (the red line in Fig. 4), only that the fall is less steep: $N_c \approx \frac{1}{\sqrt{3}}(k_B T/\mu)$. One can see that these almost empty modes are needed to allow physically important length scales and correct kinetic energy. Such a relaxation of the usual criterion of $\mathcal{O}(1)$ cutoff mode occupation has also precedents in the truncated Wigner prescription [80].

VII. CONCLUSIONS

The effectiveness of the classical field description has now been assessed across the whole 1d Bose gas, completing the campaign started in [12, 13]. Figs. 1- 2 are a synthesis of the results: the first shows the accuracy that is possible in many observables simultaneously, while the second figure specifies the cutoff that achieves this. The light orange region specifies the parameters for which accuracy is within 10% or better, and the dominant physics is indeed that of matter waves. Simulations can be confidently carried out provided the system stays in this region. Conversely, outside of this region, one or more of the standard observables are always going to be inaccurate.

Basically, there are two main regions of interest. The first is $k_B T \gtrsim \mu$, characterized by an optimal cutoff

$\text{opt}f_c = 0.64$ that depends only on temperature [13]. This result should be applicable to nonuniform gases even in a plane wave basis and covers the thermal quasicondensate, the soliton regime, and most of the degenerate gas.

The second region is the $k_B T \lesssim \mu \approx gn$ quasicondensate regime, studied here, in which quantum fluctuations are important. The optimal cutoff in this regime is $\text{opt}f_c \approx \frac{1}{3\sqrt{2\pi}}(\mu/k_B T)^{3/2}$. It lies at energies well above $k_B T$ and becomes strongly density dependent. This high cutoff is needed to correctly capture the kinetic energy held in quantum fluctuations. Importantly, it does not distort most observables, because the occupation of the additional modes is very low ($N_c \approx 18(\frac{k_B T}{\mu})^3$). This goes against the common intuition that the cutoff mode occupation should be of $\mathcal{O}(1)$.

A high cutoff here is actually a welcome result because studies of defect evolution at low temperature use very

high resolution numerical grids that have an energy cutoff well above $k_B T$, and would be suspect if $N_c \sim \mathcal{O}(1)$ was required. We can also conclude that a plane wave basis will not be accurate for nonuniform clouds whose central density exceeds $gn \gtrsim k_B T$. Bases that take into account the trap shape are then needed.

Looking forward, we have seen that the c-field variant of the extended Bogoliubov model described in Sec. III B allows one to easily reach the low temperature limit. It can also be used to investigate the case of 2d and 3d gases, which may behave very differently.

ACKNOWLEDGMENTS

This work was supported by the National Science Centre (Poland) grant No. 2012/07/E/ST2/01389.

-
- [1] M. J. Davis, T. M. Wright, P. B. Blakie, A. S. Bradley, R. J. Ballagh, and C. W. Gardiner, “C-field methods for non-equilibrium bose gases,” in *Quantum Gases* (Imperial College Press, 2013) Chap. 10, pp. 163–175.
 - [2] S. P. Cockburn and N. P. Proukakis, “The stochastic gross-pitaevskii methodology,” in *Quantum Gases* (Imperial College Press, 2013) Chap. 11, pp. 177–189.
 - [3] M. Brewczyk, M. Gajda, and K. Rzażewski, “A classical-field approach for bose gases,” in *Quantum Gases* (Imperial College Press, 2013) Chap. 12, pp. 191–202.
 - [4] T. M. Wright, M. J. Davis, and N. P. Proukakis, “Reconciling the classical-field method with the beliaev broken-symmetry approach,” in *Quantum Gases* (Imperial College Press, 2013) Chap. 19, pp. 299–312.
 - [5] J. Ruostekoski and A. D. Martin, “The truncated wigner method for bose gases,” in *Quantum Gases* (Imperial College Press, 2013) Chap. 13, pp. 203–214.
 - [6] M. Brewczyk, M. Gajda, and K. Rzażewski, *Journal of Physics B: Atomic, Molecular and Optical Physics* **40**, 023501 (2007).
 - [7] P. B. Blakie and M. J. Davis, *Journal of Physics B: Atomic, Molecular and Optical Physics* **40**, 120437 (2007).
 - [8] P. Blakie, A. Bradley, M. Davis, R. Ballagh, and C. Gardiner, *Advances in Physics* **57**, 363 (2008).
 - [9] A. S. Bradley, P. B. Blakie, and C. W. Gardiner, *Journal of Physics B: Atomic, Molecular and Optical Physics* **38**, 4259 (2005).
 - [10] M. J. Davis and P. B. Blakie, *Phys. Rev. Lett.* **96**, 060404 (2006).
 - [11] S. P. Cockburn, A. Negretti, N. P. Proukakis, and C. Henkel, *Phys. Rev. A* **83**, 043619 (2011).
 - [12] J. Pietraszewicz and P. Deuar, *Phys. Rev. A* **92**, 063620 (2015).
 - [13] J. Pietraszewicz and P. Deuar, *Phys. Rev. A* **97**, 053607 (2018).
 - [14] E. Witkowska, M. Gajda, and K. Rzażewski, *Phys. Rev. A* **79**, 033631 (2009).
 - [15] M. Brewczyk, P. Borowski, M. Gajda, and K. Rzażewski, *Journal of Physics B: Atomic, Molecular and Optical Physics* **37**, 12125 (2004).
 - [16] L. Zawitkowski, M. Brewczyk, M. Gajda, and K. Rzażewski, *Phys. Rev. A* **70**, 033614 (2004).
 - [17] A. Sinatra, C. Lobo, and Y. Castin, *Journal of Physics B: Atomic, Molecular and Optical Physics* **35**, 3599 (2002).
 - [18] S. J. Rooney, A. S. Bradley, and P. B. Blakie, *Phys. Rev. A* **81**, 023630 (2010).
 - [19] T. Sato, Y. Kato, T. Suzuki, and N. Kawashima, *Phys. Rev. E* **85**, 050105 (2012).
 - [20] S. P. Cockburn and N. P. Proukakis, *Phys. Rev. A* **86**, 033610 (2012).
 - [21] Y. Kagan and B. V. Svistunov, *Phys. Rev. Lett.* **79**, 3331 (1997).
 - [22] L. E. Sadler, J. M. Higbie, S. R. Leslie, M. Vengalattore, and D. M. Stamper-Kurn, *Nature* **443**, 312 (2006).
 - [23] C. N. Weiler, T. W. Neely, D. R. Scherer, A. S. Bradley, M. J. Davis, and B. P. Anderson, *Nature* **455**, 948 (2008).
 - [24] A. D. Martin and J. Ruostekoski, *New Journal of Physics* **12**, 055018 (2010).
 - [25] E. Witkowska, P. Deuar, M. Gajda, and K. Rzażewski, *Phys. Rev. Lett.* **106**, 135301 (2011).
 - [26] J. Sabbatini, W. H. Zurek, and M. J. Davis, *New Journal of Physics* **14**, 095030 (2012).
 - [27] T. Karpiuk, P. Deuar, P. Bienias, E. Witkowska, M. Gajda, K. Rzażewski, and M. Brewczyk, *Phys. Rev. Lett.* **109**, 205302 (2012).
 - [28] M. Gring, M. Kuhnert, T. Langen, T. Kitagawa, B. Rauer, M. Schreitl, I. Mazets, D. A. Smith, E. Demler, and J. Schmiedmayer, *Science* **337**, 1318 (2012).
 - [29] C. V. Parker, L.-C. Ha, and C. Chin, *Nature Physics* **9**, 769 (2013).
 - [30] I.-K. Liu, R. W. Pattinson, T. P. Billam, S. A. Gardiner, S. L. Cornish, T.-M. Huang, W.-W. Lin, S.-C. Gou, N. G. Parker, and N. P. Proukakis, *Phys. Rev. A* **93**, 023628 (2016).
 - [31] M. C. Tsatsos, P. E. Tavares, A. Cidrim, A. R. Fritsch, M. A. Caracanhas, F. E. A. dos Santos, C. F. Barenghi, and V. S. Bagnato, *Physics Reports* **622**, 1 (2016), quantum turbulence in trapped atomic Bose–Einstein condensates.
 - [32] S. Donadello, G. Lamporesi, G. Ferrari, S.-C. Gou, F. Dalfvo, and N. P. Proukakis, *Communications Physics* **1**, 24 (2017).
 - [33] C. N. Yang and C. P. Yang, *Journal of Mathematical Physics* **10**, 1115 (1969).

- [34] K. V. Kheruntsyan, D. M. Gangardt, P. D. Drummond, and G. V. Shlyapnikov, *Phys. Rev. A* **71**, 053615 (2005).
- [35] J. Pietraszewicz and P. Deuar, *New Journal of Physics* **19**, 123010 (2017).
- [36] C. Mora and Y. Castin, *Phys. Rev. A* **67**, 053615 (2003).
- [37] A. Sinatra, E. Witkowska, and Y. Castin, *The European Physical Journal Special Topics* **203**, 87 (2012).
- [38] S. Donadello, S. Serafini, M. Tylutki, L. P. Pitaevskii, F. Dalfovo, G. Lamporesi, and G. Ferrari, *Phys. Rev. Lett.* **113**, 065302 (2014).
- [39] S. Serafini, M. Barbiero, M. Debortoli, S. Donadello, F. Larcher, F. Dalfovo, G. Lamporesi, and G. Ferrari, *Phys. Rev. Lett.* **115**, 170402 (2015).
- [40] N. Navon, A. L. Gaunt, R. P. Smith, and Z. Hadzibabic, *Science* **347**, 167 (2015).
- [41] R. A. Duine and H. T. C. Stoof, *Phys. Rev. A* **65**, 013603 (2001).
- [42] R. J. Lewis-Swan, M. K. Olsen, and K. V. Kheruntsyan, *Phys. Rev. A* **94**, 033814 (2016).
- [43] J. Javanainen and J. Ruostekoski, *New Journal of Physics* **15**, 013005 (2013).
- [44] M. D. Lee and J. Ruostekoski, *Phys. Rev. A* **90**, 023628 (2014).
- [45] N. P. Proukakis and B. Jackson, *Journal of Physics B: Atomic, Molecular and Optical Physics* **41**, 203002 (2008).
- [46] C. W. Gardiner and M. J. Davis, *Journal of Physics B: Atomic, Molecular and Optical Physics* **36**, 14731 (2003).
- [47] C. Lobo, A. Sinatra, and Y. Castin, *Phys. Rev. Lett.* **92**, 020403 (2004).
- [48] A. S. Bradley, C. W. Gardiner, and M. J. Davis, *Phys. Rev. A* **77**, 033616 (2008).
- [49] R. N. Bisset, M. J. Davis, T. P. Simula, and P. B. Blakie, *Phys. Rev. A* **79**, 033626 (2009).
- [50] B. Damski and W. H. Zurek, *Phys. Rev. Lett.* **104**, 160404 (2010).
- [51] T. Simula, M. J. Davis, and K. Helmerston, *Phys. Rev. Lett.* **113**, 165302 (2014).
- [52] N. G. Berloff and B. V. Svistunov, *Phys. Rev. A* **66**, 013603 (2002).
- [53] N. G. Parker and C. S. Adams, *Phys. Rev. Lett.* **95**, 145301 (2005).
- [54] T. M. Wright, R. J. Ballagh, A. S. Bradley, P. B. Blakie, and C. W. Gardiner, *Phys. Rev. A* **78**, 063601 (2008).
- [55] T. Świsłocki, E. Witkowska, J. Dziarmaga, and M. Matuszewski, *Phys. Rev. Lett.* **110**, 045303 (2013).
- [56] E. Witkowska, J. Dziarmaga, T. Świsłocki, and M. Matuszewski, *Phys. Rev. B* **88**, 054508 (2013).
- [57] M. Anquez, B. A. Robbins, H. M. Bharath, M. Boguslawski, T. M. Hoang, and M. S. Chapman, *Phys. Rev. Lett.* **116**, 155301 (2016).
- [58] B. Nowak, J. Schole, D. Sexty, and T. Gasenzer, *Phys. Rev. A* **85**, 043627 (2012).
- [59] M. Schmidt, S. Erne, B. Nowak, D. Sexty, and T. Gasenzer, *New Journal of Physics* **14**, 075005 (2012).
- [60] M. Karl, B. Nowak, and T. Gasenzer, *Phys. Rev. A* **88**, 063615 (2013).
- [61] B. Nowak, J. Schole, and T. Gasenzer, *New Journal of Physics* **16**, 093052 (2014).
- [62] T. Karpiuk, M. Brewczyk, M. Gajda, and K. Rzażewski, *Journal of Physics B: Atomic, Molecular and Optical Physics* **42**, 095301 (2009).
- [63] R. J. Marshall, G. H. C. New, K. Burnett, and S. Choi, *Phys. Rev. A* **59**, 2085 (1999).
- [64] N. P. Proukakis, J. Schmiedmayer, and H. T. C. Stoof, *Phys. Rev. A* **73**, 053603 (2006).
- [65] T. Karpiuk, M. Brewczyk, M. Gajda, and K. Rzażewski, *Phys. Rev. A* **81**, 013629 (2010).
- [66] E. Witkowska, M. Gajda, and K. Rzażewski, *Optics Communications* **283**, 671 (2010).
- [67] N. N. Bogoljubov, *Journal of Physics* **XI**, No.1 (1947).
- [68] N. N. Bogoljubov, *Il Nuovo Cimento* **7** (6), 794–805 (1958).
- [69] J. Esteve, J.-B. Trebbia, T. Schumm, A. Aspect, C. I. Westbrook, and I. Bouchoule, *Phys. Rev. Lett.* **96**, 130403 (2006).
- [70] C. Sanner, E. J. Su, A. Keshet, R. Gommers, Y.-i. Shin, W. Huang, and W. Ketterle, *Phys. Rev. Lett.* **105**, 040402 (2010).
- [71] T. Müller, B. Zimmermann, J. Meineke, J.-P. Brantut, T. Esslinger, and H. Moritz, *Phys. Rev. Lett.* **105**, 040401 (2010).
- [72] T. Jacqmin, J. Armijo, T. Berrada, K. V. Kheruntsyan, and I. Bouchoule, *Phys. Rev. Lett.* **106**, 230405 (2011).
- [73] J. Armijo, T. Jacqmin, K. Kheruntsyan, and I. Bouchoule, *Phys. Rev. A* **83**, 021605 (2011).
- [74] J. Armijo, *Phys. Rev. Lett.* **108**, 225306 (2012).
- [75] A. G. Sykes, D. M. Gangardt, M. J. Davis, K. Viering, M. G. Raizen, and K. V. Kheruntsyan, *Phys. Rev. Lett.* **100**, 160406 (2008).
- [76] P. Deuar, A. G. Sykes, D. M. Gangardt, M. J. Davis, P. D. Drummond, and K. V. Kheruntsyan, *Phys. Rev. A* **79**, 043619 (2009).
- [77] P. Bienias, K. Pawłowski, M. Gajda, and K. Rzażewski, *Phys. Rev. A* **83**, 033610 (2011).
- [78] V. A. Kashurnikov, N. V. Prokof'ev, and B. V. Svistunov, *Phys. Rev. Lett.* **87**, 120402 (2001).
- [79] M. J. Davis, S. A. Morgan, and K. Burnett, *Phys. Rev. Lett.* **87**, 160402 (2001).
- [80] A. A. Norrie, R. J. Ballagh, and C. W. Gardiner, *Phys. Rev. A* **73**, 043617 (2006).

Appendix A: Accuracy of the extended Bogoliubov theory

A figure of merit for the accuracy of the Bogoliubov theory can be defined in a similar way to (21), by comparing to the exact quantum solution:

$$RMS^{(Q)}(\gamma, \tau_d) = \sqrt{(\delta_{u_G}^{(\text{Bog})})^2 + \max \left[(\delta_{\varepsilon}^{(\text{Bog})})^2, (\delta_{\varepsilon_{\text{tot}}}^{(\text{Bog})})^2 \right]}, \quad (\text{A1})$$

where

$$\delta_{\Omega}^{(\text{Bog})}(\gamma, \tau_d) = \left(\frac{\Omega^{(\text{Bog-q})}(\gamma, \tau_d)}{\Omega^{(q)}(\gamma, \tau_d)} - 1 \right). \quad (\text{A2})$$

The accurate region with less than 10% error is shown in Fig. 5 in dark blue, circumscribed by the red dashed line. We restricted our use of Bogoliubov data in the synthesis of Figs. 1 and 2 to far within this accurate region.

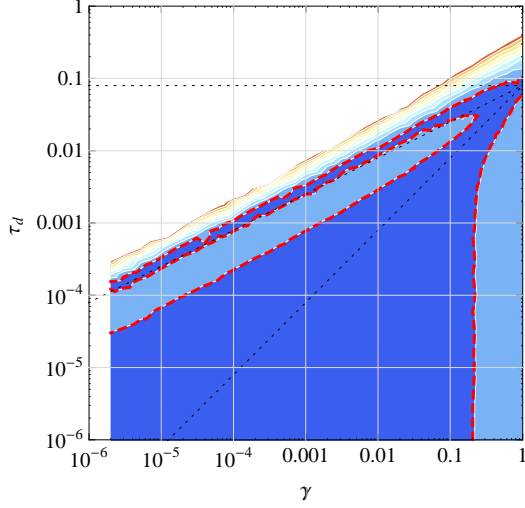


Figure 5. This diagram shows the accuracy of the extended Bogoliubov treatment with respect to exact Yang-Yang theory by plotting contours (at 0.1, 0.2, ..., 1.0) of (A1). The dark blue region together with a thick red dashed line indicates the $RMS^{(Q)} \leq 0.1$ contour.

Appendix B: Calculations with extended Bogoliubov

1. Observable expressions

Following on from Sec. III A, the fully quantum expressions for the observables are [36]:

$$g^{(2)}(z) = 1 + \frac{2}{n} \int_{-\infty}^{\infty} \frac{dk}{2\pi} [(\bar{u}_k + \bar{v}_k)^2 n_k + \bar{v}_k (\bar{u}_k + \bar{v}_k)] \cos kz, \quad (B1)$$

leading via (23) to

$$u_G = 1 + 2 \lim_{k \rightarrow 0} [(\bar{u}_k + \bar{v}_k)^2 n_k + \bar{v}_k (\bar{u}_k + \bar{v}_k)] = \frac{k_B T}{\mu}. \quad (B2)$$

This is a convenient form like (18). The interaction energy per particle continues to be related to $g^{(2)}(0)$ through (19), giving

$$\mathcal{E}_{\text{int}} = \mu - k_B T \frac{\gamma}{4\pi\tau_d}. \quad (B3)$$

The kinetic energy per particle is

$$\varepsilon = \frac{\hbar^2}{2mn} \int_{-\infty}^{\infty} \frac{dk}{2\pi} k^2 [(1 + 2\bar{v}_k^2) n_k + \bar{v}_k^2]. \quad (B4)$$

Phase correlations are

$$g^{(1)}(z) = \exp \left[-\frac{1}{n} \int_{-\infty}^{\infty} \frac{dk}{2\pi} [(\bar{u}_k + \bar{v}_k)^2 n_k + \bar{v}_k^2] (1 - \cos kz) \right]. \quad (B5)$$

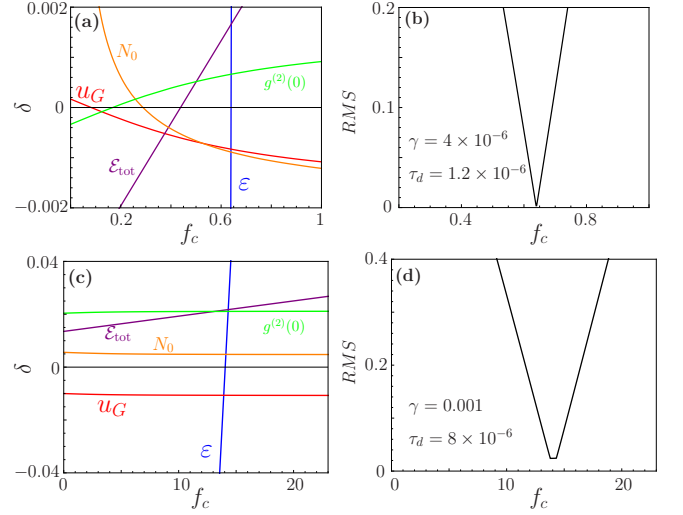


Figure 6. Cutoff dependence in the quasicondensate. The top panels are in the thermally dominated regime $\gamma = 4 \times 10^{-6}$, $\tau_d = 1.2 \times 10^{-6}$, and the lower panels in the quantum fluctuation regime $\gamma = 10^{-3}$, $\tau_d = 8 \times 10^{-6}$. Notation: $g^{(2)}(0)$ (green), u_G (red), \mathcal{E}_{tot} (purple), ε (blue), N_0 (orange). Left panels: discrepancies for single observables calculated with (22); Right panels: global discrepancy RMS calculated with (21).

For the corresponding c-field description, one has the slightly modified expression

$$g_{\text{cf}}^{(1)}(z) = \exp \left[-\frac{1}{n} \int_{-k_c}^{k_c} \frac{dk}{2\pi} (\bar{u}_k + \bar{v}_k)^2 n_k^{(\text{cf})} (1 - \cos kz) \right]. \quad (B6)$$

Consideration was also given to the condensate mode occupation, N_0 , i.e. the number of atoms in the $k = 0$ mode. This observable tends to a well defined constant value as the gas length grows, but of course it becomes negligible compared to N in the thermodynamic limit of the 1d gas. It is important for comparison to earlier cutoff determinations made in low temperature mid-size systems with $\mathcal{O}(1000)$ atoms, where condensate fraction $n_0 = N_0/N$ remained significant [14, 77]. Since the density in k space can be expressed as $\tilde{n}(k) = \frac{N}{2\pi} \int_{-\infty}^{\infty} dz g^{(1)}(z) e^{ikz}$, (B5) can be used to obtain the occupation of the lowest energy ($k \rightarrow 0$) state:

$$N_0 = \tilde{n}(0) \Delta k = n \int_{-\infty}^{\infty} dz g^{(1)}(z). \quad (B7)$$

For the c-field description, N_0 continues to be given by the form (B7) but now using $g_{\text{cf}}^{(1)}(z)$ from (B6).

2. Relative errors and optimization

The cutoff-dependent discrepancy of various observables in the quasicondensate regimes are shown in Fig. 6,

calculated using (22). We observe that ε has the the most extreme rising behavior, while u_G captures the strongest falling behavior in the vicinity where all errors are small. Hence, the best cutoff occurs at a point where there is a balance between these rising and falling predictions. The goodness of the classical field description depends on how large the actual discrepancies at this point are. The maximal error at such an optimal cutoff can be set by \mathcal{E}_{tot} or u_G .

The behavior in the quantum fluctuating condensate is somewhat similar to the behavior seen at large γ in [13], reproduced here in Fig. 7. This figure also shows a flat-bottomed minimum in RMS more clearly than in Fig. 6d because it is much broader when γ is large. For more details see Sec. D.

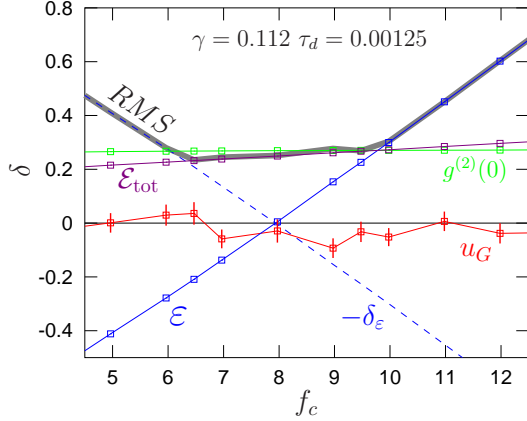


Figure 7. Cutoff dependence of the discrepancies δ_Ω for the case $\gamma = 0.112$, $\tau_d = 0.00125$ (from [13]). Notation as in Fig. 6. The figure of merit $RMS(f_c)$ is shown as the thick grey line. The dashed blue line shows $-\delta_\varepsilon$ as a reference.

In Fig. 8 one can see the results for $\min RMS$ and of_c obtained from the Bogoliubov calculations here, overlaid with the numerical ensemble results from [13]. The data analysis procedure was described in detail in [13]. For the Bogoliubov case, the data is finely spaced and smooth, and a simple application of the the Wolfram *Mathematica* algorithm `ContourPlot` turned out to be sufficient for the task, without the need for Lagrangian interpolation.

Appendix C: Kinetic energy and cutoff in the quantum fluctuation region

The exact Yang-Yang results for kinetic energy ε are shown in Fig. 9 and display a rapid increase once the regime $\gamma \gtrsim 2\pi\tau_d$ is reached. The reason for this rapid growth can be tracked to the kinetic energy present within the quantum fluctuations. To see this, let us make some approximations to (B4) in the $\mu \gg k_B T$ regime.

First, consider the thermal part that contains n_k . The main contributing modes are in the phonon regime where $E_k \approx \sqrt{2\varepsilon\mu} = \xi|k|\mu$, and their occupation can be approximated by $n_k \approx k_B T / E_k$. The quantity $\bar{v}_k^2 \approx 1/2\xi|k|$ is

much greater than one in this regime. Using all this, the thermal term in (B4) can be written as

$$\begin{aligned} \varepsilon_{\text{th}} &\approx \frac{\hbar^2}{2mn} \int_{-k_B T/\mu\xi}^{k_B T/\mu\xi} \frac{dk}{2\pi} k^2 \frac{1}{\xi|k|} \frac{k_B T}{\xi|k|\mu} = \left(\frac{k_B T}{\mu}\right)^2 \frac{\mu}{2\pi\xi n} \\ &\approx \frac{k_B T \tau_d}{\sqrt{\gamma}} \end{aligned} \quad (\text{C1})$$

The other part of (B4) (the quantum fluctuation term) contains just \bar{v}_k^2 . This quantity decays rapidly $\bar{v}_k^2 \approx 1/(k\xi)^4$ in the particle regime, and has negligible contribution there. Hence, just the phonon contribution is relevant. The crossover in the behavior of \bar{v}_k to particle-like is at $|k| = 2^{1/3}/\xi$, so the quantum fluctuation part is

$$\varepsilon_{\text{qf}} \approx \frac{\hbar^2}{2mn} \int_{-2^{1/3}/\xi}^{2^{1/3}/\xi} \frac{dk}{2\pi} k^2 \frac{1}{2\xi|k|} = \frac{\mu}{2^{5/3}\pi n \xi} \approx \frac{k_B T \gamma^{3/2}}{4\pi^2 2^{2/3} \tau_d} \quad (\text{C2})$$

This is far larger than (C1), and indicates that kinetic energy is indeed dominated by quantum fluctuations.

Let us now see what happens in the c-field description. The expression (20) contains only a thermal term, but $n_k^{(\text{cf})} = k_B T / E_k$ does not decay as fast as in a Bose-Einstein distribution and both phonon-like and particle-like modes contribute. Using again the crudest useful approximation, the phonon and particle regimes meet at $|k| = 2/\xi$. Taking the leading terms,

$$\begin{aligned} \varepsilon^{(\text{cf})} &\approx \frac{\hbar^2}{mn} \left\{ \int_0^{2/\xi} \frac{dk}{2\pi} k^2 \frac{1}{\xi|k|} \frac{k_B T}{\xi|k|\mu} + \int_{2/\xi}^{k_c} \frac{dk}{2\pi} k^2 \frac{2k_B T}{\mu(\xi k)^2} \right\} \\ &= \frac{k_B T k_c}{\pi n} \left(1 - \frac{1}{f_c} \sqrt{\frac{\mu}{2\pi k_B T}} \right) \\ &\approx \frac{k_B T k_c}{\pi n} = 2k_B T f_c \sqrt{\tau_d}. \end{aligned} \quad (\text{C3})$$

The second term in the brackets on the 2nd line turns out to be small once the estimate (C4) is obtained. The estimate (C3) corresponds to assuming exactly $k_B T$ purely kinetic energy per mode. Since the vast majority of modes are particle-like because of the high cutoff, this is actually a reasonable approximation.

(C3) can be compared to the quantum kinetic energy (C2). Such a comparison gives the following prediction for the cutoff based on kinetic energy alone:

$$f_c \approx 0.008 \left(\frac{\gamma}{\tau_d} \right)^{\frac{3}{2}}. \quad (\text{C4})$$

(C4) agrees remarkably well with the Bogoliubov result (25) and the exact numerics.

Appendix D: Bogoliubov estimates for $\text{opt } f_c$ and $\min RMS$ in the quantum fluctuating regime

The quantum fluctuating Bogoliubov regime has two small parameters: $\gamma \ll 1$ and a temperature scaled with

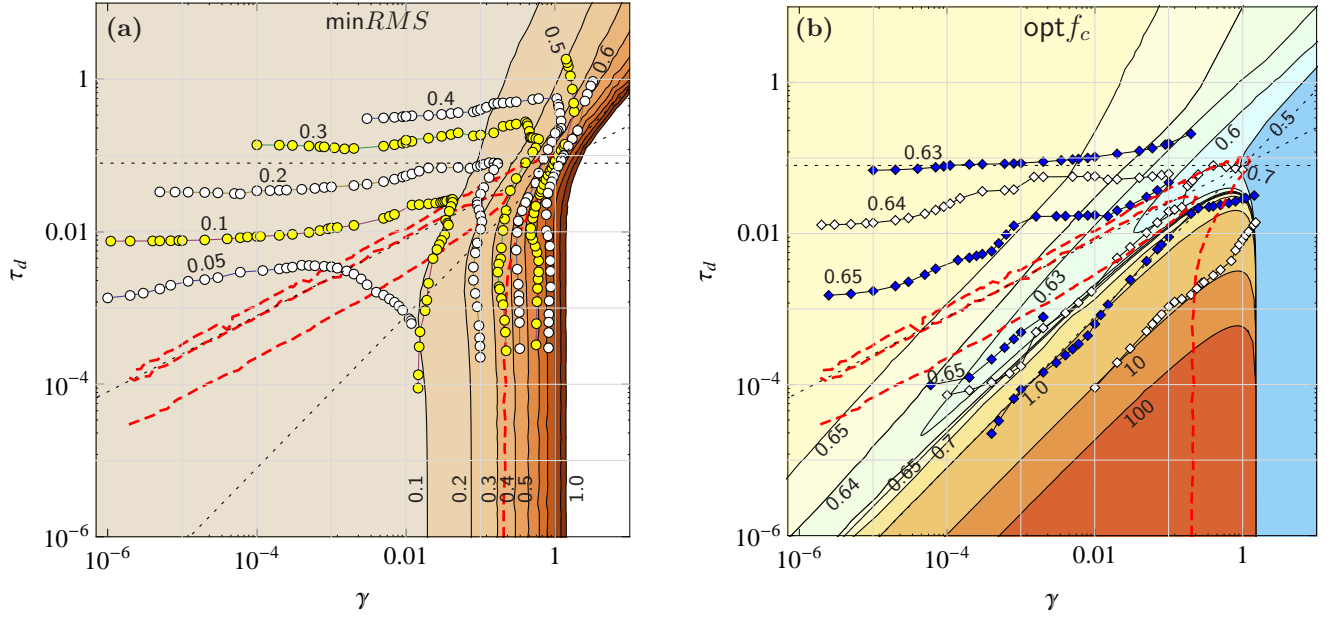


Figure 8. A detailed comparison of raw Bogoliubov and numerical ensemble results. Contours of $\min RMS$ (a) and $\text{opt } f_c$ (b) are shown with numbered values on the plot, similarly to Figs. 1 and 2, respectively. Bogoliubov results are shown as solid contours between colored fields, while contours derived from the numerical ensembles [13] are shown as joined symbols. The red dashed line is copied from Fig. 5 and shows the location at which the error between the Bogoliubov and exact results reaches 10%.

respect to the chemical potential:

$$t = \frac{2\pi\tau_d}{\gamma} \approx \left(\frac{k_B T}{\mu} = u_G \right) \ll 1. \quad (\text{D1})$$

The equality $k_B T/\mu = u_G$ follows from (B2) and (18). We will make a self-consistent expansion of the required quantities in these small parameters. We know from (C4) that the scaling $\text{opt } f_c \propto t^{-3/2}$ holds in this regime, which will be confirmed in (D21). Assuming that we will be working in the vicinity of $\text{opt } f_c$, it is required to take this scaling into account to preserve terms of the right order in the expansion. Therefore, we define the prefactor p_c

via

$$f_c = \frac{p_c}{t^{3/2}}. \quad (\text{D2})$$

1. Chemical potential and related quantities

To obtain an approximation to μ , the equation of state (9) is first evaluated to the form

$$\frac{1}{t} = \frac{1}{u_G} + \frac{1}{\pi} \sqrt{\frac{\gamma}{t u_G}} \left[1 - \frac{\pi^2 u_G^2}{12} + \frac{\pi^4 u_G^4}{48} - \frac{\pi^6 u_G^6}{32} + \mathcal{O}(u_G^8) \right]. \quad (\text{D3})$$

In detail, the integral in (9) can be written as

$$- \frac{T}{2\pi\sqrt{\mu}} \int_0^\infty ds \left[\frac{s}{R(e^{sR\sqrt{2/u_G}} - 1)} + \frac{s - R\sqrt{2/u_G}}{2R} \right] \quad (\text{D4})$$

with $R = \sqrt{1 + \frac{1}{2}s^2 u_G} = \sqrt{1 + \Delta(s)}$. While the second term easily integrates, the first does not. However, the $[e^{sR\sqrt{2/u_G}} - 1]^{-1}$ factor cuts out any contributions at large $s \gtrsim \sqrt{u_G/2}$. Since $u_G \ll 1$, then Δ takes on small values $\Delta \lesssim \frac{1}{4}u_G^2 \ll 1$, and $R \approx 1$. The first term in the integrand of (D4) can be written as a MacLaurin series in $r(s) = R - 1 \ll 1$ as $\sum_j M_j(s)r(s)^j$. Its integration is still troublesome beyond the lowest terms, so $r(s)$ is further expanded in the small quantity $s^2 u_G/4$ like $r =$

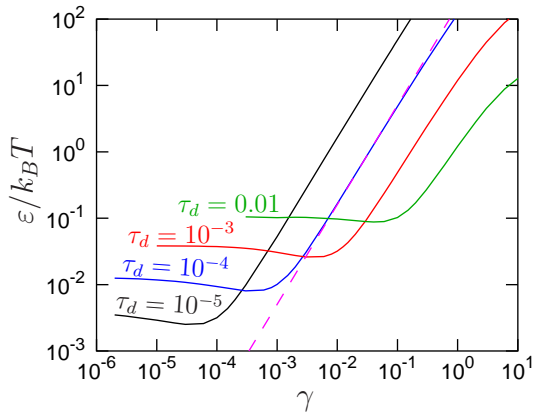


Figure 9. Kinetic energy ϵ as a function of γ . Exact Yang-Yang results. The magenta dashed line shows the approximation (C2) for $\tau_d = 10^{-4}$.

$\frac{s^2 u_G}{4} - \frac{s^4 u_G^2}{32} + \dots$. This then gives the following series

$$- \frac{T}{2\pi\sqrt{\mu}} \sum_{jj' > 0} \int_0^\infty ds \mathcal{T}_{jj'}(s) \left(\frac{s^2 u_G}{4} \right)^{j'} + \frac{\sqrt{\gamma}}{\pi\sqrt{t u_G}}, \quad (\text{D5})$$

in which all the integrals give (D3). We spare the reader from explicit expressions for the $\mathcal{T}_{jj'}$.

Now, to obtain a self-consistent expansion for μ , we postulate an ansatz

$$\mu = \frac{k_B T}{t} \sum_{j,j' \geq 0} c_{jj'} t^j \gamma^{j'/2} \quad (\text{D6})$$

with coefficients $c_{jj'}$ to be determined. By equating subsequent terms of the same orders of $\sqrt{\gamma}$ and t appearing in (D3) one obtains the following series expansion:

$$\begin{aligned} \frac{\mu}{k_B T} = \frac{1}{t} & \left[1 - \frac{\sqrt{\gamma}}{\pi} + \frac{\gamma}{2\pi^2} - \frac{\gamma\sqrt{\gamma}}{8\pi^3} \right] \\ & + \frac{t\sqrt{\gamma}\pi}{12} \left[1 + \frac{\sqrt{\gamma}}{\pi} + \frac{3\gamma}{8\pi^2} \right] \mathcal{O}(t^3, \gamma^2). \end{aligned} \quad (\text{D7})$$

For c-fields, the integral in (15) can be expressed as

$$\frac{1}{t} = \frac{1}{u_G^{(\text{cf})}} - \frac{\sqrt{\gamma t u_G^{(\text{cf})}}}{\pi} \tan^{-1} \left[f_c \sqrt{\frac{\pi u_G^{(\text{cf})}}{2}} \right], \quad (\text{D8})$$

and the resulting series expansion is

$$\begin{aligned} \frac{\mu^{(\text{cf})}}{k_B T} = \frac{1}{t} & + \frac{\sqrt{\gamma}}{2} \left[1 - \frac{t\sqrt{8}}{p_c \pi^{3/2}} + \frac{4t^3 \sqrt{2}}{3\pi^{5/2} p_c^3} \right] - \frac{\gamma t}{8} \left[1 - \frac{t\sqrt{8}}{\pi^{3/2} p_c} \right] \\ & + \frac{5\gamma^{3/2} t^2}{64} \left[1 - \frac{8\sqrt{8}t}{5\pi^{3/2} p_c} \right] + \mathcal{O}(t^4, \gamma^2). \end{aligned} \quad (\text{D9})$$

The leading correction terms in (D7) and (D9), of $\mathcal{O}(\sqrt{\gamma})$, have the opposite sign and no cutoff dependence. This proves what was previously found empirically: no cutoff choice will match chemical potentials exactly in the quantum fluctuating regime. Since all of u_G , $\mathcal{E}_{\text{int}} = T/u_G - T/2t$ and $g^{(2)}(0) = 2t\mathcal{E}_{\text{tot}}/T = (2t/u_G) - 1$ depend simply on μ and the control parameters γ and τ_d , they will *never be exactly matched* by any cutoff. The leading order terms for the various observable estimates (which may be of use for future work) are:

$$u_G = t \left[1 + \frac{\sqrt{\gamma}}{\pi} + \frac{\gamma}{2\pi^2} \right] - \frac{\pi t^3 \sqrt{\gamma}}{12} \left[1 + \frac{3\sqrt{\gamma}}{\pi} \right] + \mathcal{O}(t^5, t\gamma^{3/2}) \quad (\text{D10})$$

$$u_G^{(\text{cf})} = t - \frac{t^2 \sqrt{\gamma}}{2} + t^3 \left[\frac{\sqrt{2\gamma}}{\pi^{3/2} p_c} + \frac{3\gamma}{8} \right] + \mathcal{O}(t^4, \gamma^2) \quad (\text{D11})$$

$$\begin{aligned} g^{(2)}(0) = 1 - \frac{2\sqrt{\gamma}}{\pi} + \frac{\gamma}{\pi^2} - \frac{\gamma^{3/2}}{4\pi^3} + \frac{\pi t^2 \sqrt{\gamma}}{6} \left[1 + \frac{\sqrt{\gamma}}{\pi} \right] \\ + \mathcal{O}(t^4, t^2 \gamma^{3/2}, \gamma^2) \end{aligned} \quad (\text{D12})$$

$$\begin{aligned} g^{(2)}(0)^{(\text{cf})} = 1 + t\sqrt{\gamma} - t^2 \sqrt{\gamma} \left[\frac{\sqrt{8}}{\pi^{3/2} p_c} + \frac{\sqrt{\gamma}}{4} \right] \\ + t^3 \gamma \left[\frac{1}{\sqrt{2}\pi^{3/2} p_c} + \frac{5\sqrt{\gamma}}{32} \right] + \mathcal{O}(t^4, \gamma^2). \end{aligned} \quad (\text{D13})$$

2. Kinetic energy

The integral (B4) can be reduced to integrable terms in the same way as the one in (9). Upon substituting (D7) and keeping consistent orders, we obtain

$$\begin{aligned} \frac{\varepsilon}{k_B T} = \frac{\sqrt{\gamma}}{3\pi t} \left[1 - \frac{3\sqrt{\gamma}}{2\pi} + \frac{9\gamma}{8\pi^2} + \frac{\pi^2 t^2}{4} \left(1 + \frac{\sqrt{\gamma}}{\pi} + \frac{3\gamma}{8\pi^2} \right) \right] \\ + \mathcal{O}(t^3, \gamma^2). \end{aligned} \quad (\text{D14})$$

The integral in (20) can be performed, so

$$\frac{\varepsilon^{(\text{cf})}}{k_B T} = \sqrt{\frac{2\gamma t}{\pi}} \left(f_c - \frac{1}{\sqrt{2\pi u_G^{(\text{cf})}}} \tan^{-1} \left[f_c \sqrt{\frac{\pi u_G^{(\text{cf})}}{2}} \right] \right). \quad (\text{D15})$$

This leads to the following expressions:

$$\begin{aligned} \frac{\varepsilon^{(\text{cf})}}{k_B T} = \frac{p_c \sqrt{2\gamma}}{t\sqrt{\pi}} - \frac{\sqrt{\gamma}}{2} + \frac{t\sqrt{2\gamma}}{\pi^{3/2} p_c} - \frac{t\gamma}{8} + \frac{3t^2 \gamma}{p_c \sqrt{8\pi^3}} \\ + \mathcal{O}(t^3, t^2 \gamma^{3/2}, \gamma^2) \end{aligned} \quad (\text{D16})$$

with the discrepancy

$$\begin{aligned} \delta_\varepsilon = 3p_c \sqrt{2\pi} - 1 + \frac{9p_c \sqrt{\gamma}}{\sqrt{2\pi}} + \frac{27p_c \gamma}{4\sqrt{2}\pi^{3/2}} - t^2 \frac{3(p_c^2 \pi^3 - 4)}{p_c \sqrt{8\pi}} \\ - \frac{3\pi t}{2} \left[1 + \frac{3\sqrt{\gamma}}{2\pi} + \frac{9\gamma}{8\pi^2} \right] + \mathcal{O}(t^2 \sqrt{\gamma}, \gamma^{3/2}, t^3). \end{aligned} \quad (\text{D17})$$

Equating this to zero gives the optimum cutoff for kinetic energy (only):

$$f_c^{(\varepsilon)} = \frac{1}{3\sqrt{2\pi} t^{3/2}} \left[1 - \frac{3\sqrt{\gamma}}{2\pi} + \frac{9\gamma}{8\pi^2} + \frac{3\pi t}{2} + \mathcal{O}(t^2, \gamma^{3/2}) \right]. \quad (\text{D18})$$

One can see that the leading factor of (D18) when converted to γ, τ_d variables is $f_c^{(\varepsilon)} = \frac{1}{12\pi^2} (\gamma/\tau_d)^{3/2} (1 + \dots)$. The prefactor $\frac{1}{12\pi^2} = 0.00844$ is a remarkably close match to that seen in (C4). To include the other observables and get an estimate for minRMS , analysis of the full RMS figure of merit is necessary.

3. Analytic optimization

The discrepancy for total energy is

$$\begin{aligned} \delta_{\mathcal{E}_{\text{tot}}} = \sqrt{\gamma} \left[\frac{4}{3\pi} + 2p_c \sqrt{\frac{2}{\pi}} - \frac{\pi t^2}{3} \right] + \gamma \left[\frac{16}{9\pi^2} + \frac{8\sqrt{2}p_c}{3\pi^{3/2}} \right] \\ - t^2 \gamma \left(\frac{31}{18} + \frac{2p_c \sqrt{2\pi}}{3} \right) + \mathcal{O}(t^3, \gamma^{3/2}). \end{aligned} \quad (\text{D19})$$

Zeroing out the leading term requires negative p_c , but p_c must be positive and was assumed $\mathcal{O}(1)$, so $\delta_{\mathcal{E}_{\text{tot}}}$ is always positive in the vicinity of the optimum cutoff that interests us. In fact, $\delta_{\mathcal{E}_{\text{tot}}} \approx 2\sqrt{\gamma}/\pi$ at the $f_c^{(\varepsilon)}$ cutoff.

As a corollary to the above, the term $\mathcal{M} = \max[\delta_\varepsilon^2, \delta_{\mathcal{E}_{\text{tot}}}^2]$ in (21) must take on the flat-bottomed shape seen in Fig. 6(c). The ends of the flat-bottomed part will occur when $\delta_{\mathcal{E}_{\text{tot}}} = \pm\delta_\varepsilon$, i.e when

$$f_c^\pm = \frac{1}{3\sqrt{2\pi}t^{3/2}} \left[1 + \frac{(\pm 4 - 3)\sqrt{\gamma}}{2\pi} + \frac{(59 \mp 32)\gamma}{24\pi^2} + \frac{3\pi t}{2} \pm t\sqrt{\gamma} + \frac{(4 \mp 1)\gamma t}{6\pi} + \mathcal{O}(\gamma^{3/2}, t^2) \right] \quad (\text{D20})$$

When the full $RMS(f_c)$ in the flat bottom region is constructed, we have $RMS^2 = \delta_{u_G}^2 + \delta_{\mathcal{E}_{\text{tot}}}^2 = \gamma(\frac{25}{9\pi^2} +$

$\frac{16\sqrt{2}p_c}{3\pi^{3/2}} + \frac{8p_c^2}{\pi} + \mathcal{O}(t, \sqrt{\gamma}))$. The leading order of this always has positive gradient with f_c . This implies that the leftmost edge corresponds to the overall minimum of $\min RMS$, i.e. $\text{opt} f_c = f_c^-$,

$$\text{opt} f_c = \frac{1}{3\sqrt{2\pi}t^{3/2}} \left[1 - \frac{7\sqrt{\gamma}}{2\pi} + \frac{91\gamma}{24\pi^2} + \frac{3\pi t}{2} - t\sqrt{\gamma} + \frac{5\gamma t}{6\pi} + \mathcal{O}(t^2, \gamma^{3/2}) \right]. \quad (\text{D21})$$

The global figure of merit at this point is

$$\min RMS = \frac{\sqrt{5\gamma}}{\pi} \left[1 + \frac{\sqrt{\gamma}}{30\pi} + \frac{\pi t}{2} + \frac{\sqrt{\gamma}t}{6} - t^2 \left(6 + \frac{\pi^2}{12} \right) + \gamma \frac{1889}{1800\pi} + \mathcal{O}(t\gamma, t^2\sqrt{\gamma}, \gamma^{3/2}, t^2) \right]. \quad (\text{D22})$$